Research Article

Alexander Battig, Naïssa Abdou-Rahaman Fadul, Daniele Frasca, Dietmar Schulze, and Bernhard Schartel*

Multifunctional graphene nanofiller in flame retarded polybutadiene/chloroprene/carbon black composites

https://doi.org/10.1515/epoly-2021-0026
received January 28, 2021; accepted February 25, 2021

Abstract: To curtail flammability risks and improve material properties, flame retardants (FRs) and fillers are mixed into rubbers. High loadings of aluminum trihydroxide (ATH) and carbon black (CB) are the most used FRs and reinforcing additive, respectively, in rubbers. To reduce loading without losing mechanical properties, partial substitution of ATH as well as CB by low amounts of multilayer graphene (MLG) nanoparticles is investigated. The high aspect ratio MLG is made of ten graphene sheets. In polybutadiene/chloroprene (BR/CR) nanocomposites 3 phr MLG replaced 15 phr CB and/or 3 phr ATH. Material and mechanical properties as well as fire behavior of the nanocomposites are compared to BR/CR with 20 phr CB both with and without 50 phr ATH. MLG appears as a promising nanofiller to improve the functional properties: replacement of CB improved rheological, curing, and mechanical properties; substitution of ATH improved nanocomposite properties without affecting flame retardancy.

Keywords: nanocomposites, rubbers, multilayer graphene, carbon black, polybutadiene/chloroprene

1 Introduction

Rubber materials are widely employed due to their valuable material properties; however, as synthetic polymers, they are flammable and can burn with high fire loads, which can ultimately lead to catastrophic damage and loss of life in case of accidental fire. Flame retardant (FR) additives are commonplace for synthetic polymers, especially rubbers; in many cases the rigid filler content is greater than 40 parts per hundred rubber (phr). Their implementation serves two main functions: for one, the additives improve mechanical properties such as Young's modulus or hardness and alter gas-barrier properties of the rubber (1–3). Moreover, fillers replace a portion of the matrix, substituting combustible fuel with less volatile or non-flammable material. FR additives are crucial for highly flammable materials such as rubbers, which burn with dense smoke production, to protect them from fire and ignition sources. Common fillers are silica and carbon black (CB). For all reinforcing fillers, their efficacy in improving properties depends on their aspect ratio, their adhesion to the matrix, as well as their dispersion, orientation, and concentration in the rubber.

A major drawback to conventional fillers such as CB is the relatively high loading needed to yield desirable properties, which is why nanofillers are particularly interesting alternatives: nanoparticles reinforce elastomers at lower loadings due to their larger surface area and better aspect ratio compared to fillers such as CB. Previous investigations have proven the efficacy of nanofillers at low loadings, thereby demonstrating improvements in mechanical and flame-retardant properties: examples include the use of modified clay (4,5), silica (6,7), carbon nanotubes (8,9), and graphene (10–12). Moreover, the use of multilayer graphene (MLG) has been proven as an effective multifunctional filler for polyvinyl alcohol–polyaniline hydrogels (13), acrylonitrile–butadiene–styrene (14), chlorine–isobutyl–isoprene, hydrogenated acrylonitrile–butadiene, nitrile–butadiene, styrene–butadiene, and natural rubbers (15–19). However, MLG's ability to function in polybutadiene/chloroprene (BR/CR) has not been accurately described.

Polybutadiene/chloroprene is a blend of polybutadiene, which is non-polar, and polychloroprene, a polar polymer. Polybutadiene is among the most widely used

* **Corresponding author: Bernhard Schartel,** Bundesanstalt für Materialforschung und -prüfung (BAM), Unter den Eichen 87, 12205 Berlin, Germany, e-mail: bernhard.schartel@bam.de
Alexander Battig, Naïssa Abdou-Rahaman Fadul, Daniele Frasca, Dietmar Schulze: Bundesanstalt für Materialforschung und -prüfung (BAM), Unter den Eichen 87, 12205 Berlin, Germany

synthetic rubbers worldwide and the second most produced behind styrene butadiene rubber. Polychloroprene, commonly called by its trade name "Neoprene" given by DuPont, is a synthetic elastomer of repeating 2-chlorobuta-1,3-diene monomers; its structure is thereby closely related to 1,3-butadiene, the monomer of BR. The high demand of BR stems from its material and mechanical properties, which is why most of its production is consumed for the manufacture of pneumatic tires (20). BR is used as a toughening agent to improve the impact resistance of other polymers such as polychloroprene, for which the main areas of application are in protective clothing, electrical insulation, as membranes, in medical devices, and as adhesives. Notably, it exhibits better flame retardancy compared to strictly hydrocarbon-based rubbers (21). The global market size of BR was $10.8 billion in 2019 and expected to rise to $13.8 billion by 2024 (22), while the global market size of polychloroprene reached approx. 384 thousand metric tons in 2019, and is expected to rise to about 500 thousand metric tons by 2024 (23). The high market impact of these materials makes improving their safety all the more crucial.

This study investigates the use of MLG, which is usually called graphene, in multicomponent rubber blends based on BR with CR (BR/CR) and its effects on the mechanical and flame-retardant properties. MLG is composed of about ten graphene sheets, it has an aspect ratio of 40, and a theoretical BET (Brunauer–Emmett–Teller) surface of approx. 250 $m^2\ g^{-1}$; the BET parameter is linked to the degree of exfoliation of the graphite (24,25). It is commercially available and produced via the thermal exfoliation of graphite, known as the Hummer method (15). The flame-retardant properties of MLG arise from its improvement of the protection layer effect. Previous investigations have highlighted MLG's ability to partially replace metal hydrate FRs such as aluminum trihydroxide (ATH) (16,19,26). Moreover, several investigations into synergistic combinations of nanoparticles and conventional FRs have been proposed successfully, particularly plate-like nanoparticles together with metal hydrates (27–33). Nonetheless, ATH remains a staple for industrial applications, as it is a common, i.e., inexpensive (approx. US $0.50 kg^{-1}), inorganic FR additive which functions via the release of water and its endothermic decomposition in fires, as well as the replacement of combustible material (34). The major drawback is it requires high loadings (>40%) to afford effective flame retardancy performance, thus strongly impacting mechanical properties. Therefore, the continued investigation of MLG to lower the ATH content and potentially replace CB as a reinforcing filler is of great interest.

In this study, a mixture with 20 phr CB serves as a reference for BR/CR with a conventional filler, and a specimen with additional 50 phr of precipitated ATH serves as the reference for a flame-retarded material. These BR/CR composites are compared to MLG-containing nanocomposite rubbers with various loadings in terms of curing and mechanical properties as well as FR performance. In two formulations, MLG is investigated as a replacement for CB, in FR- and non-FR-containing formulations, respectively. In other formulations, MLG is examined as a replacement for 3 phr ATH, and additionally, MLG is tested as a substitute for 3 phr ATH and 15 phr CB. These formulations investigate the potential for MLG to act as a multicomponent filler, able to not only substitute CB as a reinforcing filler but also ATH as an effective FR, and thus lower the filler content without sacrificing material properties. The efficacy of MLG in BR/CR signals the ability

Table 1: Rubber compound formulations, given in per hundred rubber (phr)

	BR/CR/CB20	BR/CR/ATH50/CB20	BR/CR/MLG3/CB5	BR/CR/ATH50/MLG3/CB5	BR/CR/ATH47/MLG3/CB20	BR/CR/ATH47/MLG3/CB5
BR	30	30	30	30	30	30
CR	70	70	70	70	70	70
CB N660	20	20	5	5	20	5
ATH	—	50	—	50	47	47
MLG	—	—	3	3	3	3
Zinc oxide	3.5	3.5	3.5	3.5	3.5	3.5
Stearic aid	2.0	2.0	2.0	2.0	2.0	2.0
Vulcacit Thiuram C	1.0	1.0	1.0	1.0	1.0	1.0
DPG	1.0	1.0	1.0	1.0	1.0	1.0
Sulfur	1.0	1.0	1.0	1.0	1.0	1.0

of this component to act in a broad range of rubber materials and highlights its versatility as an alternative to conventional fillers.

2 Materials and methods

Polybutadiene rubber (BR) (Buna CB 1220), zinc oxide (Zinkoxyd aktiv), and Vulcacit Thiuram C were supplied by Lanxess Deutschland GmbH (Germany). Polychloroprene rubber (CR) (BAYPREN 110 M49) was purchased from Arlanxeo Deutschland GmbH (Germany). 1,3-Diphenylguanidine (DPG) (Rhenocure DPG) was bought from Rhein Chemie Rheinau GmbH (Germany). Precipitated ATH (APYRAL 200 SM; particle size ca. 0.8 µm) was supplied by Nabaltec AG (Germany), and CB (Corax N 660) was purchased from Orion Engineered Carbons GmbH (Germany). Stearic acid was supplied by Baerlocher GmbH (Germany). Sulfur was purchased from Merck KGaA (Germany). MLG (EXG R98 250; BET = 250 $m^2 g^{-1}$) was produced by Graphit Kropfmühl AG (Germany). It was prepared into a masterbatch according to the method described by Frasca et al. (15) using an UPS 400 S ultrasonication lance (Hielscher Ultrasonics GmbH, Germany) and applying a 7:1 ratio of BR:MLG. Toluene of analytical grade used for this process was purchased from Chemsolute, Th. Geyer GmbH & Co. KG (Germany). The solvent was evaporated in a rotary evaporator (Hei Vap Value, Heidolph Instruments GmbH & Co. KG, Germany).

Table 1 describes the formulations of the investigated rubber compounds. All rubber samples were prepared by compounding in a two-roll mill (Lab Walzwerk MT 6″ × 13″; Rubicon Gummitechnik und Maschinenbau GmbH, Germany), with a roll temperature set at 50°C. The speed was set at 19 rpm with a friction ratio of 1:1:1. First, BR and CR were mixed with zinc oxide, stearic acid, Vulcacit Thiuram C, and CB. ATH was additionally added for the respective samples in this step. For MLG-containing formulations, the masterbatch was added in a second step. In the final mixing step, DPG and sulfur were added to the mill, and the total mixing time was 20 min. Sheets with varying thickness (2, 3, and 6 mm) were cured at 160°C at a pressure of 300 bar in a compression mold. The vulcanization time was adjusted to the respective plate thickness.

All vulcanization parameters such as maximum and minimum of torque (MH and ML, respectively) and curing time (t_{90}) were determined using a Dynamic Moving Die Rheometer (D-MDR 3000, MonTech Werkstoffprüfmaschinen GmbH, Germany). It was operated isothermally at 160°C at 1.66 Hz and 0.5°. The same machine was used to measure the storage modulus (G') and the dynamic viscosity (η') of a 5 g sample of the uncured material as a function of frequency (strain amplitude = 1%, T = 100°C), and as a function of amplitude (f = 1 Hz, T = 60°C).

The storage modulus (G') and dynamic loss factor (tan δ) as functions of temperature of the cured rubbers were determined using a MCR 501 Rheometer (Anton Paar GmbH, Austria) at a temperature range from −80°C to 70°C, a heating rate of 1 K min^{-1}, and a strain amplitude of 0.1% at a frequency of 1 Hz.

Five type 2 dumbbell samples (2 mm thickness) were used to perform tensile tests according to ISO 37. Using a stress–strain machine (Zwick/Roell Z010 instrument; ZwickRoell GmbH & Co. KG, Germany), three type 5A dumbbell samples (2 mm thickness) were used to determine Young's modulus according to ISO 527 series. A set of three (3) samples (6 mm thickness) were used to measure Shore A hardness according to ISO 7619-1.

The electrical resistance was measured with a Fischer Tera-Ohmmeter TO-3 (H.-P. FISCHER ELEKTRONIK GmbH & Co. Industrie und Labortechnik KG, Mittenwalde, Germany) and a guard ring electrode type FE 50 with an inner diameter of 50 mm. The tested samples were 3 mm thick. The specific electrical resistance was determined according to ISO 14309.

Micrograph images of freeze-fractured gold-coated surfaces were taken using a scanning electron microscope (SEM; Zeiss EVO MA 10; Carl Zeiss AG, Germany) set to an acceleration voltage of 10 kV.

Micrograph images of 200 and 70 nm thick cryo microtome sections (T = −100°C; Ultracut UCT, Leica, Wetzlar, Germany) were used for investigations with a transmission electron microscope (TEM; JEM-2200FS; JEOL Ltd., Japan) set to an acceleration voltage of 200 kV.

Two reaction-to-small-flame tests were performed: limiting oxygen index (LOI) tests were completed according to ISO 4589-2 using an FTT (East Grinstead, UK) instrument on specimens sized 112 mm × 6.5 mm × 3 mm. UL-94 measurements were done in accordance with IEC 60695-11-10 on specimens sized 120 mm × 13 mm × 3 mm. Forced flaming well-vented fire behavior measurements were conducted on a cone calorimeter (FTT, East Grinstead, UK) according to ISO 5660 on specimens sized 100 mm × 100 mm × 3 mm, using a heat flux of 50 kW m^{-2}. Although the standard stipulates a distance of 25 mm between radiator and sample, a 35 mm distance was used, as the heat flux distribution is not significantly impacted (35). As several flame-retardant formulations exhibited strong deformation during initial cone calorimeter tests, the samples were fastened using two 0.6 mm metal wires across the surface and placed into a retainer frame.

3 Results and discussion

3.1 Morphology of rubber composites

Figure 1 shows the SEM micrographs of the freeze-fractured surfaces of the BR/CR nanocomposites: Figure 1a displays BR/CR/CB20, Figure 1b displays BR/CR/ATH50/CB20, and Figure 1c shows BR/CR/MLG3/CB5, while Figure 1d displays BR/CR/ATH50/MLG3/CB5, Figure 1e corresponds to BR/CR/ATH47/MLG3/CB20 and Figure 1f belongs to BR/CR/ATH47/MLG3/CB5. The fillers are well dispersed in the polymer matrix since no agglomerates are present on the rubbers' surface. The incorporation of 3 phr MLG resulted in a rougher surface with more protuberances, both when it replaced 15 phr CB and 3 phr ATH. The increase in roughness is attributed to the stronger interactions between MLG and the matrix, compared to CB, and the presence of protuberances to MLG particles wrapped by a layer of rubber (36). The addition of 50 phr ATH gave a smoother surface to BR/CR/CB20 and BR/CR/MLG3/CB5.

The images in the left column of Figure 2 display TEM images of rubber nanocomposites (approx. 2.5 μm × 2.5 μm areas), and the right column exhibits TEM images at higher magnification (approx. 1.0 μm × 1.0 μm). In Figure 2a, the TEM image of BR/CR/MLG3/CB5 highlights the presence of MLG as thin, thread-like streaks, and CB as darker spots sized between 80 and 150 nm. Notably, the MLG stacks are clearly exfoliated, as their thickness is only several nanometers, implying that MLG formed homogenous nanocomposites. This is more closely exemplified by Figure 2b, where the dark streaks show MLG stacks only several nanometers in thickness, as well as CB particles sized approx. 200 nm in diameter. Figure 2c and e displays the ATH-containing rubber nanocomposites BR/CR/ATH47/MLG3/CB20 and BR/CR/ATH47/MLG3/CB5, respectively. The ATH-crystal distribution highlights a well-dispersed (sub-)micro-composite; they are indicated by the large, elongated rectangular shapes sized between 300 and 800 nm, which is consistent with the supplier details for the particle size (d_{10} = 0.3 μm, d_{50} = 0.4 μm, d_{90} = 0.8 μm). Interestingly, regions rich in MLG form

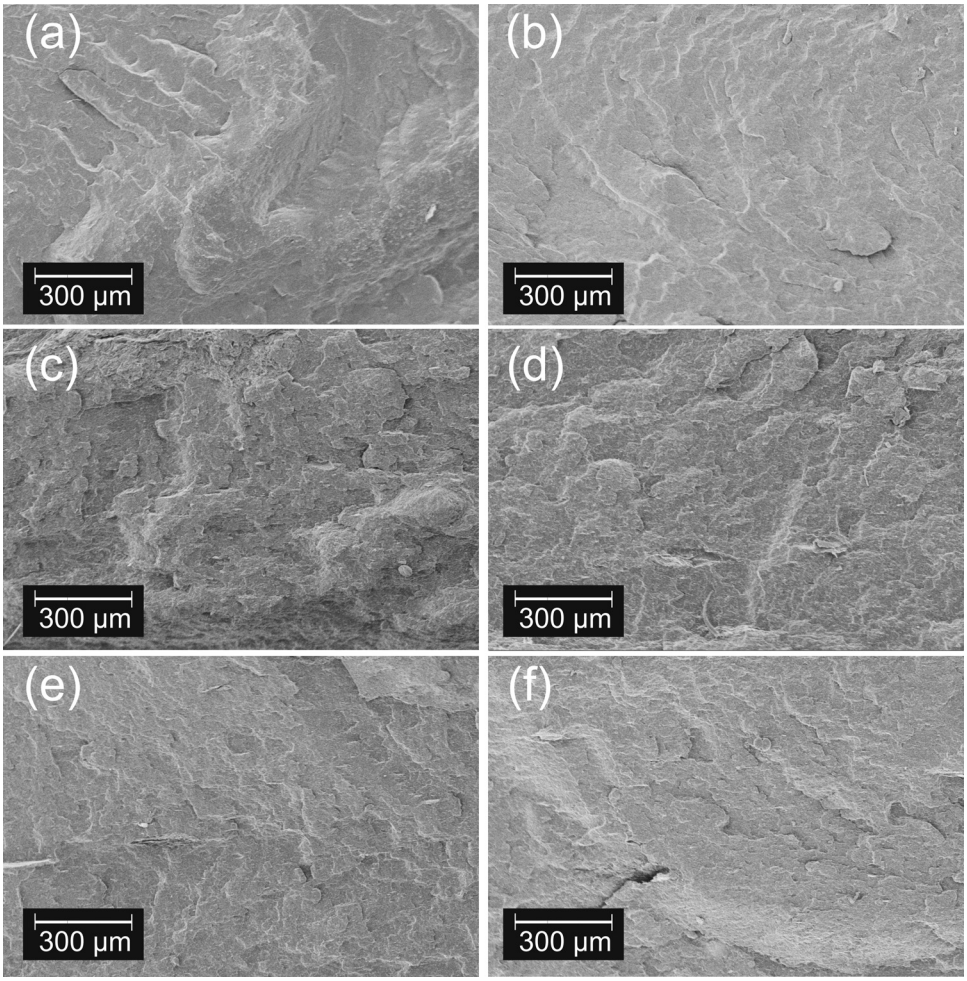

Figure 1: SEM micrographs of BR/CR rubber nanocomposites; (a) BR/CR/CB20, (b) BR/CR/ATH50/CB20, (c) BR/CR/MLG3/CB5, (d) BR/CR/ATH50/MLG3/CB5, (e) BR/CR/ATH47/MLG3/CB20, (f) BR/CR/ATH47/MLG3/CB5.

separate and distinct sections, implicating that MLG does not agglomerate around other compounds in the rubber matrix. Although the samples themselves are homogenously mixed, MLG and ATH formed discrete regions throughout the material; however, these regions are only between 0.3 and 1.0 µm in size. Figure 2d and e further highlights the distinct regions of MLG and ATH/CB and further illuminates MLG's high degree of exfoliation and homogenous distribution without agglomeration.

3.2 Rheology of uncured BR/CR composites

Rheological investigations of uncured rubber mixtures were conducted using a dynamic moving die rheometer in two operating modes: in one, the strain amplitude was held constant at 1% at 100°C while the frequency was varied (frequency sweep; Figure 3), and in the other, the frequency was held constant at 1 Hz at 60°C, while the strain amplitude was varied (amplitude sweep; Figure 4). Generally, frequency sweeps help to characterize the time-dependent behavior of a sample, while amplitude sweeps aim at characterizing the deformation behavior. Information on the dispersion of fillers may also be gained from frequency and amplitude sweeps.

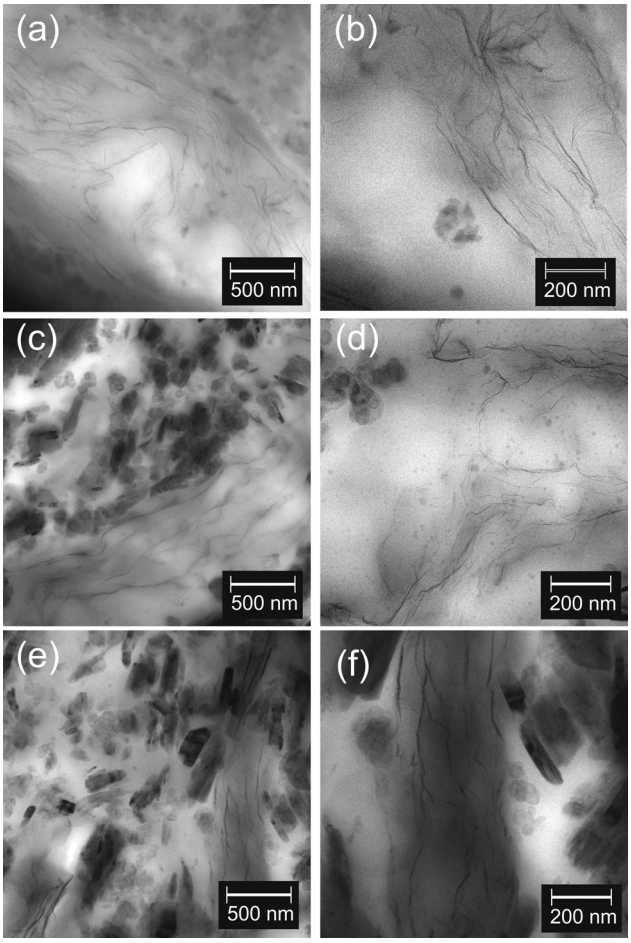

Figure 2: TEM images of BR/CR rubber nanocomposites at 8,000× (left column) and at 20,000× magnification (right column), (a + b) BR/CR/MLG3/CB5, (c + d) BR/CR/ATH47/MLG3/CB20, and (e + f) BR/CR/ATH47/MLG3/CB5.

Figure 3 displays the results from rheological measurements of uncured rubber composites at variable frequencies. Frequency sweeps are useful to gain insight into the dispersion of fillers in uncured rubber systems (17). Figure 3a plots the storage modulus (G') as a function of frequency, and Figure 3c presents the dynamic viscosity (η') over the frequency, both in logarithmic scales. The rubber composites displayed an increase of G' with increasing frequency in Figure 3a, as the elastic properties became more dominant. Correspondingly, η' decreased with increasing frequency in Figure 3c, as the viscous behavior became less pronounced. The addition of fillers such as ATH and MLG led to higher G' and η' values for all rubber compounds because their addition reinforces and increases the elastic properties of the rubber, and their presence led to higher shear stress (and thus higher viscosity). This effect was more clearly distinguishable at low frequencies, and Figure 3b and d displays G' and η', respectively, at a frequency of 0.25 Hz over the filler content. Both graphs highlight similar trends: 3 phr MLG were able to replace the five-fold amount of CB in BR/CR composites, as both BR/CR/MLG3/CB5 and BR/CR/ATH50/MLG3/CB5 exhibited increased or equal G' and η' values compared to those mixtures with 20 phr CB, thus illustrating the reinforcing effect of MLG and its efficacy at lowering filler content without loss of material properties. The addition of ATH generally led to increased storage moduli and dynamic viscosities, especially the replacement of 3 phr ATH with 3 phr MLG in BR/CR/ATH47/MLG3/CB20 strongly increased G' and η' compared to the other composites and particularly BR/CR/ATH50/CB20, although the filler content remained unchanged at 70 phr.

The results from amplitude sweeps of uncured BR/CR composites are presented in Figure 4. Figure 4a plots G' as a function of the logarithmic amplitude, while Figure 4b shows the difference of initial and final G' ($\Delta G'$) over the filler content. In Figure 4a, all materials trended toward a lower boundary for high amplitudes, i.e., similar G' values; conversely, G' increased and became disparate for all materials with decreasing amplitude, a phenomenon known as the Payne effect, which is attributed to alterations to the microstructure of the material induced

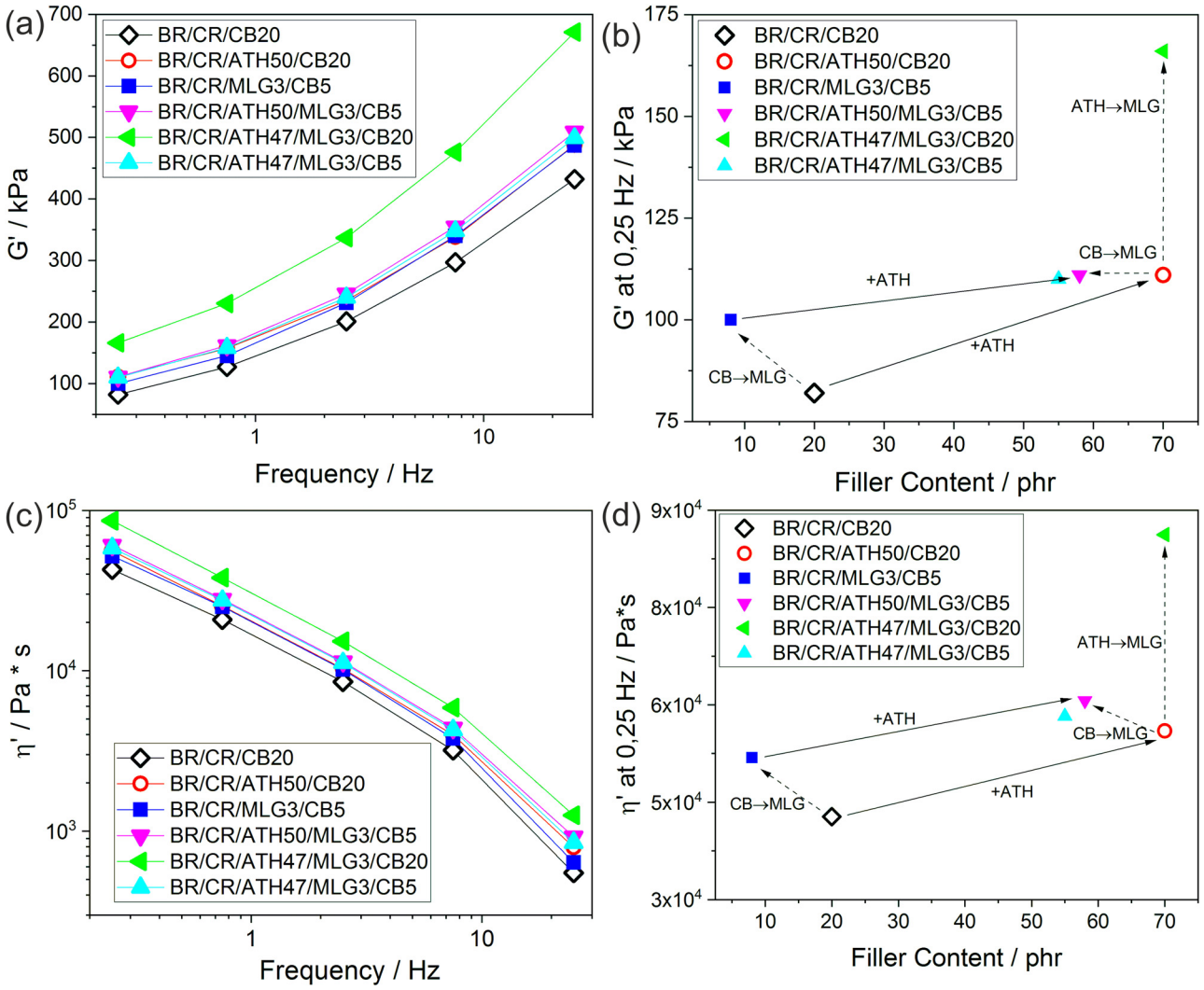

Figure 3: Rheology of uncured rubber composites: frequency sweep; (a) storage modulus over frequency, (b) storage modulus at 0.25 Hz vs filler content, (c) dynamic viscosity over frequency, and (d) dynamic viscosity at 0.25 Hz vs filler content. For (b) and (d): solid line is the addition of 50 phr of ATH; dashed line is the substitution of 15 phr CB with 3 phr MLG, or 3 phr ATH with 3 phr MLG, respectively.

by deformations (37). The formation of filler networks became more apparent with decreasing amplitudes: BR/CR/CB20 attained the lowest G' value of all materials at low frequencies, and higher storage moduli were obtained for materials containing ATH or MLG or a combination of both; BR/CR/ATH47/MLG3/CB20 had the highest value for G' at lowest frequencies. The behavior is further exemplified in Figure 4b, where $\Delta G'$ is plotted vs filler content. The changes in $\Delta G'$ of the individual rubber formulations followed the same trend seen in frequency sweeps: the addition of ATH increased $\Delta G'$, as did the replacement of CB with MLG. The replacement of 3 phr ATH with 3 phr MLG in BR/CR/ATH47/MLG3/CB20 showed the best viscoelastic properties, i.e., highest $\Delta G'$. Particularly noteworthy is that the composite BR/CR/ATH47/MLG3/CB5 attained a nearly equal $\Delta G'$ value compared to BR/CR/ATH50/CB20; here, the viscoelastic properties of the latter were almost identical to the former, but at 15 phr lower loading.

3.3 Curing properties of BR/CR composites

Figure 5a exhibits the curing curves of BR/CR composites in torque versus time, Figure 5b the minimum (ML) and Figure 5c maximum (MH) torque, and Figure 5d plots the difference between ML and MH (ΔS) over filler content of the rubber composites. The curing curves in Figure 5a showcase that the vulcanization process led to increased torque over time for all composites, thereby confirming the cross-linking reaction between sulfur and the elastomeric chain. All materials reached their maximum torque

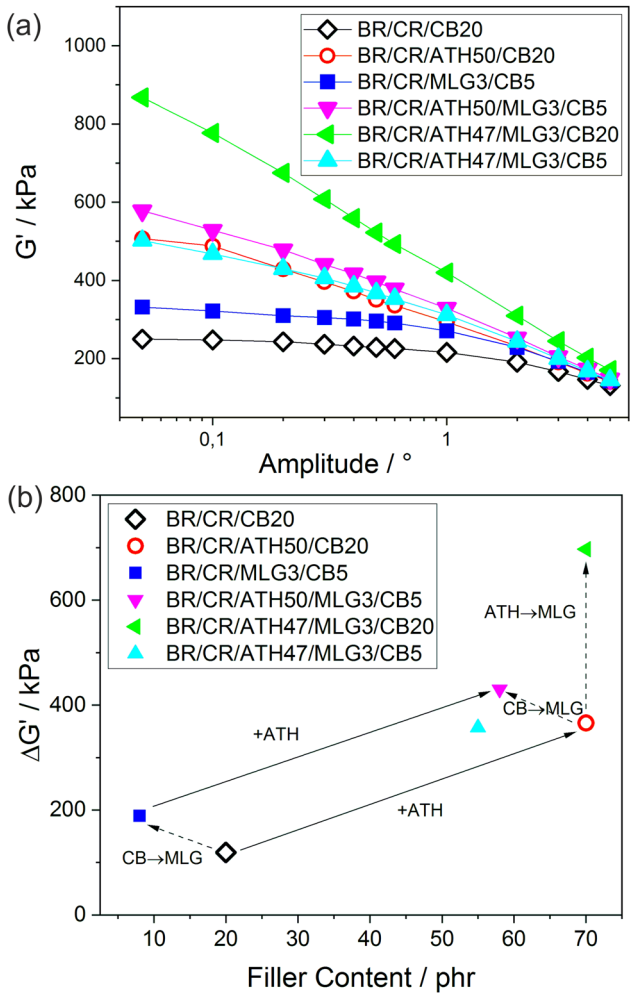

Figure 4: Rheology of uncured rubber composites: amplitude sweep; (a) storage modulus as a function of strain amplitude, (b) difference between initial and final storage modulus vs filler content. For (b): solid line is addition of 50 phr ATH; dashed line is the substitution of 15 phr CB with 3 phr MLG, or 3 phr ATH with 3 phr MLG, respectively.

after about 8 min. Greater insight is gained by comparing the scorch times (t_{s1}), which is a parameter that characterizes the start of vulcanization (induction period): when comparing the values in Table 2, all compounds attained lower t_{s1} values compared to the reference material BR/CR/CB20, pointing to an accelerated reaction among sulfur, accelerator, and activator (38). More specifically, the addition of ATH greatly reduced scorch times, as BR/CR/ATH50/CB20 attained the lowest t_{s1} value. However, the MLG-containing nanocomposite also exhibited similar t_{s1} values to BR/CR/ATH50/CB20. These results imply that although ATH was the largest contributor to reducing the induction time, the MLG nanocomposites achieved similar results at lower loadings, illustrating the ability of MLG to replace ATH and especially CB.

The stock modulus is related to the maximum torque (39) and an increase in maximum torque (MH) signifies an increased reinforcing effect and overall improvement of mechanical properties (40). Figure 5c displays the maximum torque over filler content for all rubber composites. The material BR/CR/CB20 had an MH of 13.9 dNm, and the addition of 50 phr ATH (BR/CR/ATH50/CB20) increased this value to 20.3 dNm (46% increase), due to the rigid nature of the inorganic additive. Notably, BR/CR/ATH47/MLG3/CB20, the composite where 3 phr ATH were replaced with 3 phr MLG, displayed the highest MH at 25.0 dNm (80% increase). BR/CR/MLG3/CB5, the nanocomposite with the lowest overall loading as 15 phr CB were replaced with 3 phr MLG, displayed an increase of 0.5 dNm compared to BR/CR/CB20, indicating the good reinforcing quality of MLG. The addition of ATH to the nanocomposite (BR/CR/ATH50/MLG3/CB5) also increased MH to a level similar to BR/CR/ATH50/CB20, namely to 19.5 dNm (40% increase). Interestingly, the MH of the nanocomposite BR/CR/ATH47/MLG3/CB5, where MLG replaces both a portion of ATH and three quarters of CB, was not greatly reduced (18.7 dNm) compared to the compound with 50 phr ATH, further highlighting the capabilities of MLG as a multifunctional nanofiller.

The changes in the minimum of torque (ML) are shown in Figure 5b. ML is related to the viscosity of the uncured system (41). The graph illustrates a similar trend to MH measurements: the addition of ATH led to higher ML values, and the replacement of 15 parts CB with 3 phr MLG also yielded higher ML values. Particularly, BR/CR/ATH47/MLG3/CB5 attained ML values almost equal to those of BR/CR/ATH50/CB20 but did so at lower loadings. The results agree with rheology measurements of the uncured material. Figure 5d shows the difference of maximum and minimum torque (ΔS) over filler content; ΔS is considered proportional to the crosslink density (42,43). The changes in ΔS of the varying composites follow the same pattern seen for MH and ML.

3.4 Mechanical properties of BR/CR rubber composites: tensile tests

The results from tensile tests of the cured rubber composites are presented in Figure 6 and are summarized in Table 3: the typical stress–strain curves are displayed in Figure 6a, and Figure 6b–e plots the stress at 100% (Figure 6b) or 200% elongation (Figure 6c), or the tensile strength (Figure 6d) and elongation at break (Figure 6e) over the filler content.

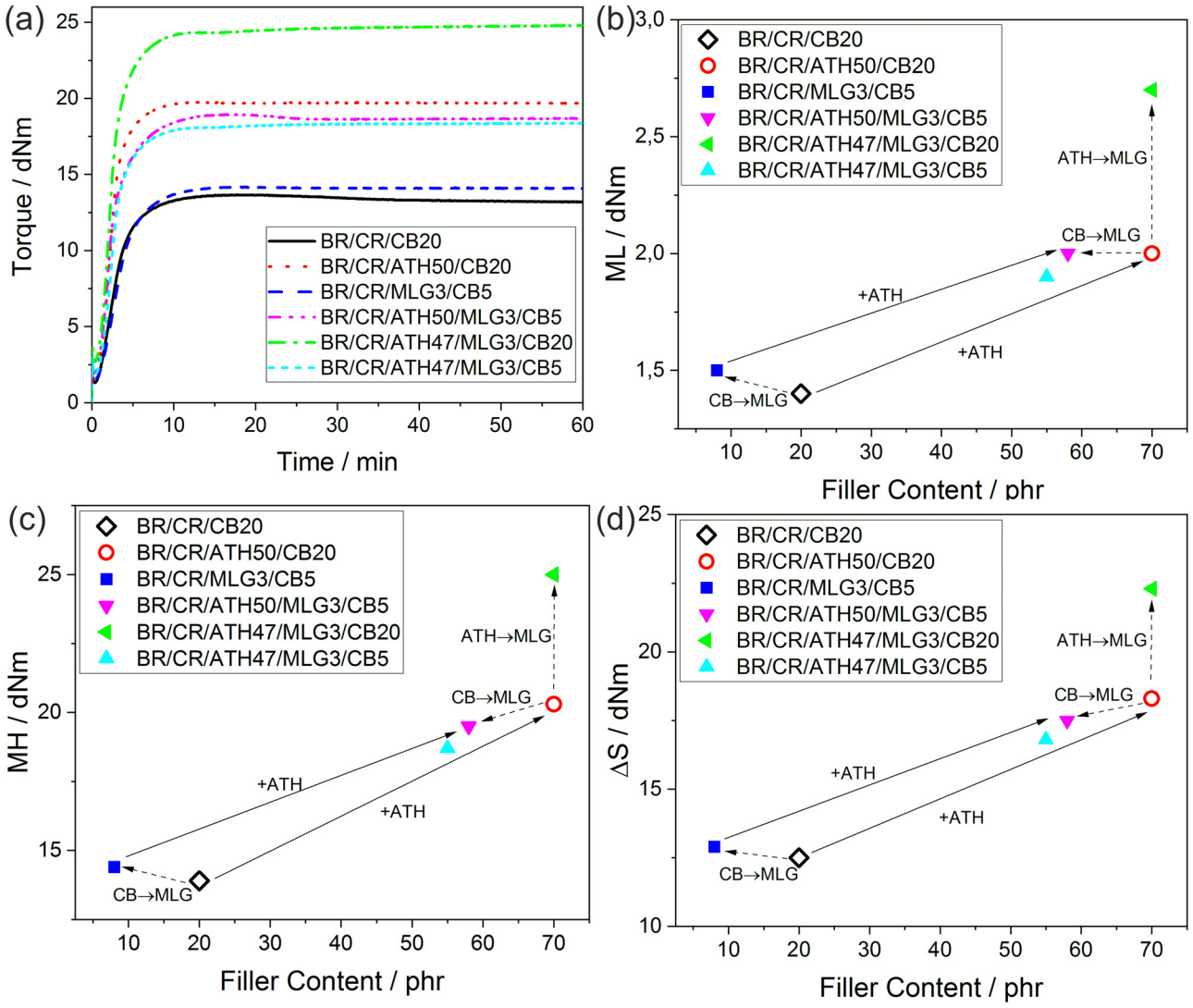

Figure 5: Curing properties of BR/CR composites: (a) curing curves, i.e., torque over time, (b) minimum of torque (ML) vs filler content of composites, (c) maximum of torque (MH) vs filler content, and (d) difference between maximum and minimum of torque (ΔS) vs filler content. For (b), (c), and (d): solid line is addition of 50 phr ATH; dashed line is replacement of 15 phr CB with 3 phr MLG, or 3 phr ATH with 3 phr MLG, respectively.

Table 2: Curing characteristics of BR/CR rubber composites

	BR/CR/CB20	BR/CR/ATH50/CB20	BR/CR/MLG3/CB5	BR/CR/ATH50/MLG3/CB5	BR/CR/ATH47/MLG3/CB20	BR/CR/ATH47/MLG3/CB5
t_{s1} (min)	1.4 ± 0.2	1.1 ± 0.1	1.3 ± 0.1	1.0 ± 0.1	1.0 ± 0.1	1.2 ± 0.1
t_{s2} (min)	1.7 ± 0.3	1.4 ± 0.1	1.8 ± 0.2	1.2 ± 0.1	1.2 ± 0.1	1.5 ± 0.1
t_{90} (min)	7.2 ± 0.6	5.7 ± 0.7	7.8 ± 0.5	7.1 ± 0.5	6.5 ± 0.5	6.7 ± 0.7

The addition of ATH or MLG increased stress at lower elongation but led to a decrease in elongation at break for all rubbers. The graphs in Figure 6 highlight the changes of BR/CR composites when fillers are added: compared to BR/CR/CB20, the addition of 50 phr ATH in BR/CR/ATH50/CB20 led to increased stress at 100% and 200% elongation, yet the effect was less pronounced at the latter elongation; moreover, the tensile strength increased slightly and the elongation at break slightly decreased. When MLG was incorporated in the rubbers,

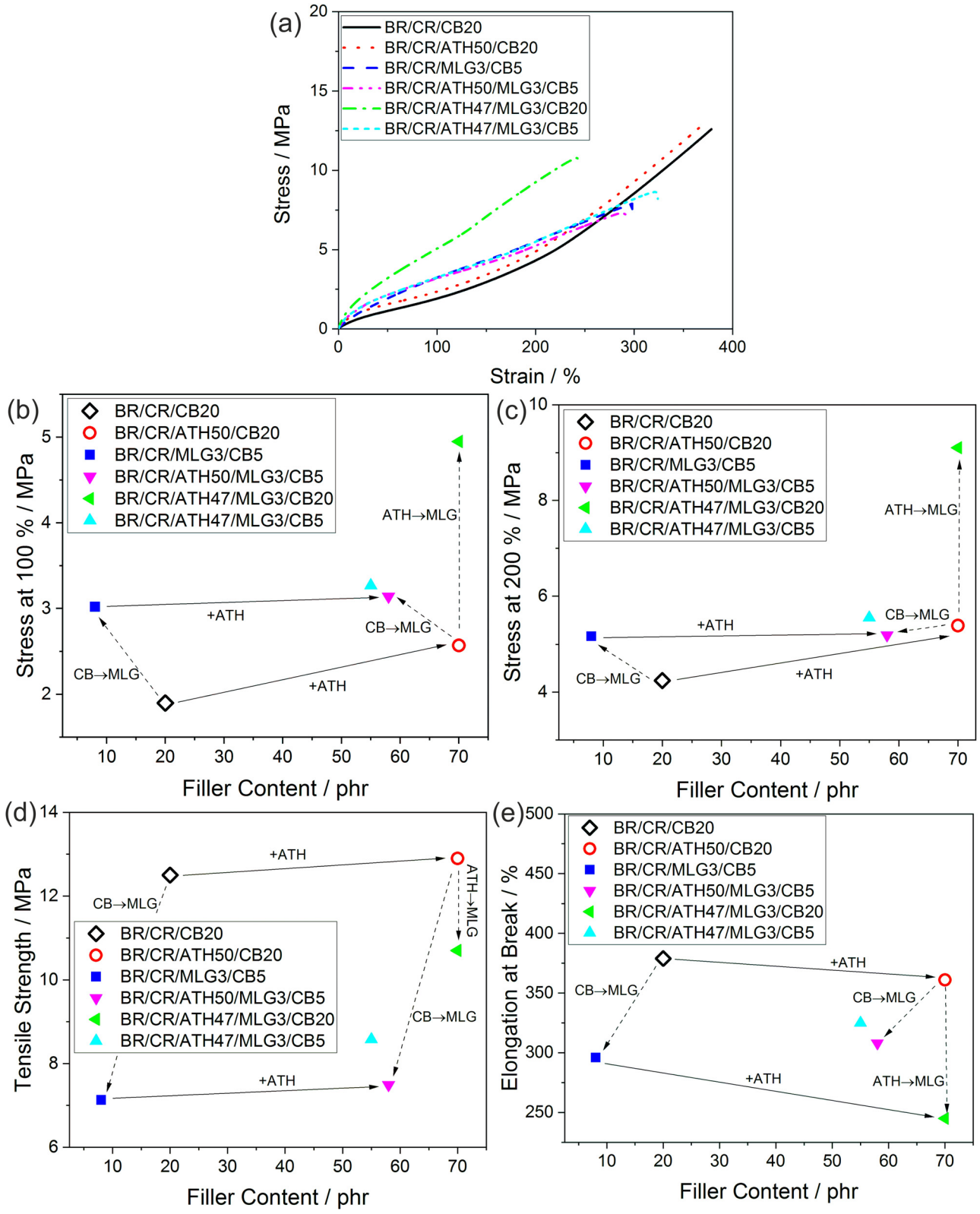

Figure 6: Results from tensile tests of cured BR/CR rubber composites; (a) tensile stress vs strain curves, (b) stress at 100% elongation and (c) at 200% elongation vs filler content, (d) tensile strength and (e) elongation at break vs filler content. For b, c, d, and e: solid line is addition of 50 phr ATH, dashed line is the replacement of 15 phr CB with 3 phr MLG, or 3 phr ATH with 3 phr MLG.

Table 3: Mechanical properties of BR/CR composites

	BR/CR/CB20	BR/CR/ATH50/CB20	BR/CR/MLG3/CB5	BR/CR/ATH50/MLG3/CB5	BR/CR/ATH47/MLG3/CB20	BR/CR/ATH47/MLG3/CB5
Elongation at break (%)	393 ± 19	369 ± 16	296 ± 22	294 ± 21	250 ± 16	329 ± 8
Young's modulus (MPa)	4.27 ± 0.1	16.5 ± 0.4	6.1 ± 0.1	20.5 ± 1.3	29.5 ± 0.5	18.8 ± 0.8
Hardness (Shore A)	56.2 ± 0.2	65.9 ± 0.5	60.2 ± 0.5	66.7 ± 0.6	74.1 ± 0.3	66.9 ± 0.4
Tensile strength (MPa)	12.6 ± 0.9	13.0 ± 1.1	7.6 ± 0.8	7.3 ± 0.6	11.0 ± 0.7	8.9 ± 0.4
Stress at 100% (MPa)	1.9 ± 0.1	2.6 ± 0.2	3.1 ± 0.2	3.2 ± 0.1	5.0 ± 0.1	3.3 ± 0.1

tensile strength and elongation at break were highly reduced. The stresses at 100% and 200% elongation of BR/CR/MLG3/CB5 (lowest filler content) were nearly identical to those with significantly higher filler contents, such as BR/CR/ATH50/CB20 and BR/CR/ATH50/MLG3/CB5. Although BR/CR/MLG3/CB5 exhibited low tensile strength, the mixture BR/CR/ATH47/MLG3/CB5 displayed an elongation at break almost equal to BR/CR/20 and BR/CR/ATH50/CB20.

Stress at 100% elongation as a function of filler content is shown in Figure 6b. When used in replacement of CB or ATH, MLG led to higher stress values. The substitution of 15 phr CB with 3 phr MLG increased the stress at 100% elongation by 62% for BR/CR/MLG3/CB5 and by 23% for BR/CR/ATH50/MLG3/CB5. The most notable stress increase was obtained in BR/CR/ATH47/MLG3/CB20 with the replacement of ATH by MLG: the stress at 100% was improved by 92% compared to BR/CR/ATH50/CB20. The addition of ATH in the rubber composites increased the stress value for BR/CR/ATH50/CB20 by 35% and did not change the stress value for BR/CR/ATH50/MLG3/CB5. At 200% elongation, the same pattern was revealed for the rubber composites, except for BR/CR/ATH50/MLG3/CB5 where 15 phr CB were substituted by 3 phr MLG, which led to a slight decrease in stress (Figure 6c).

Figure 6d shows the tensile strength over filler content. The use of MLG in the BR/CR rubbers caused crucial tensile strength losses of 15%, 39%, and 44%, respectively, for BR/CR/ATH47/MLG3/CB20, BR/CR/MLG3/CB5, and BR/CR/ATH50/MLG3/CB5. The incorporation of ATH kept the tensile strength of the BR/CR rubbers constant. The elongation at break over filler content is displayed in Figure 6e. The presence of another filler in the BR/CR/CB rubber composites led to a high decrease of elongation at break. The losses are more important for substitutions with MLG than the addition of ATH.

Figure 7a displays the stress–strain curves at low strains which were used to determine Young's modulus (E), and Figure 7b plots Young's modulus over filler content. Figure 7 further highlights the changes to the material with the addition of fillers: both MLG and ATH improve Young's modulus, resulting in stiffer rubbers. This phenomenon correlates well with SEM images, where an increased surface roughness was determined

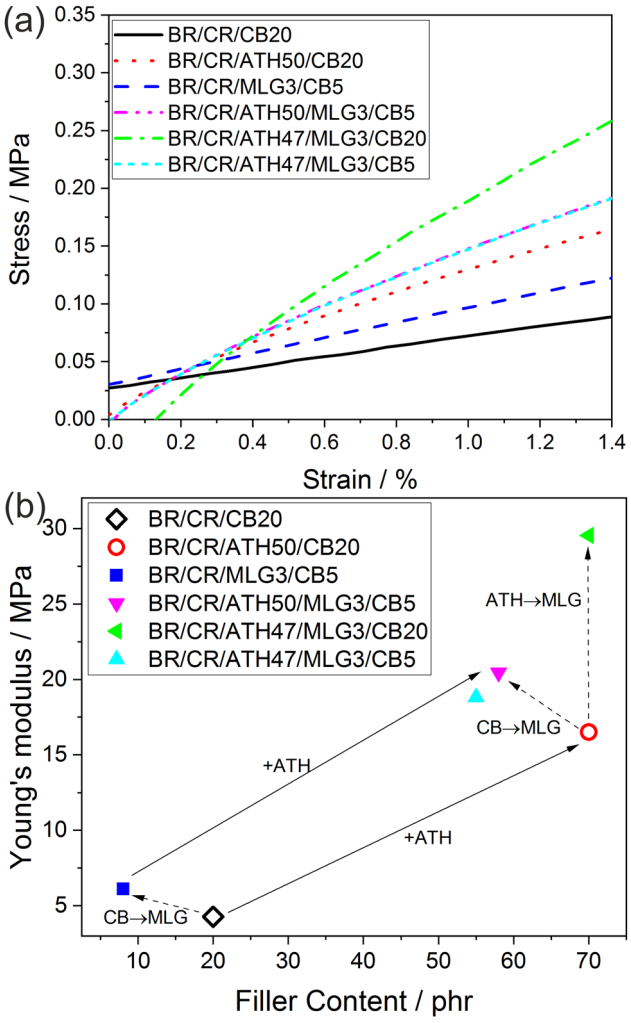

Figure 7: Tensile tests of cured BR/CR rubber composites; (a) stress–strain curve at low stresses, used to determine Young's modulus and (b) Young's modulus of the BR/CR composites vs filler content.

for ATH and MLG containing materials; higher surface roughness is attributed to increased stiffness, i.e., Young's modulus (44–46). The incorporation of 50 phr ATH greatly increased E: the value for BR/CR/ATH50/CB20 was nearly four times higher (387% increase) than that of BR/CR/CB20, and E of BR/CR/ATH50/MLG3/CB5 was three times higher (334%) compared to that of BR/CR/MLG3/CB5. All MLG containing compounds displayed higher Young's moduli compared to their non-MLG containing counterparts. The substitution of 15 phr CB with 3 phr MLG increased E by over 40% for BR/CR/MLG3/CB5 and by 24% for BR/CR/ATH50/MLG3/CB5. Moreover, the substitution of 3 phr ATH with 3 phr MLG in BR/CR/ATH47/MLG3/CB20 led to a Young's modulus nearly 80% higher compared to BR/CR/ATH50/CB20.

Generally, MLG acted as a strengthening filler for BR/CR composites in terms of mechanical stability. The materials with MLG showcased reduced tensile strengths and elongation at break, as well as an increased stress at elongations and Young's modulus; the materials became more brittle due to the structural properties of MLG. This behavior is connected to the formation of crosslinked network in the rubber matrix (42,43) and the reduced interactions of MLG with the rubber due to polar groups. In fact, the ratio of non-polar groups is significant in the rubber: CR contains chlorine and makes 70% of the rubber in weight. The best improvement of mechanical properties was obtained in BR/CR/ATH47/MLG3/CB20, with the substitution of 3 phr ATH by 3 phr MLG. Young's modulus, hardness, and stress at 100% elongation are improved (+13 MPa; +8 Shore A and +2.37 MPa) but the tensile strength is lower (−2 MPa) and the elongation at break is worse than the other rubber composites (−120%). This shows a synergetic effect between ATH, MLG, and CB with the ratio ATH47/MLG3/CB20.

3.5 Mechanical properties of BR/CR rubber composites: shore hardness tests and dynamic mechanical properties

Figure 8a exhibits the hardness of BR/CR composites as a function of filler content. Hardness was both improved by adding ATH in high amounts and replacing 15 phr CB and/or 3 phr ATH with 3 phr MLG. By substituting 15 phr CB with 3 phr MLG, a higher hardness was obtained with lower filler content. When comparing BR/CR/CB20 to BR/CR/MLG3/CB5, although the filler content was lower by a factor of 2.5, the hardness increased by four Shore A. This higher hardness value is explained by the better packing density obtained when MLG is used with CB (47). The addition of ATH in the reference rubber BR/CR/CB20 showed the best improvement of hardness caused by the substantial amount of filler added: BR/CR/ATH50/CB20 hardness was higher by 9.7 Shore A compared to BR/CR/CB20. The hardness of BR/CR/MLG3/CB5 was also improved by the addition of ATH (increase of 6.5 Shore A). At high loadings, replacing 3 phr ATH with 3 phr MLG resulted in an increase of eight Shore A with the same amount of filler content (BR/CR/ATH50/CB20 and BR/CR/ATH47/MLG3/CB20). This improvement was also due to the better packing density obtained with ATH, CB, and MLG blended together in the rubber matrix. When 15 phr CB was replaced by 3 phr MLG in the presence of ATH, the obtained hardness was slightly higher (by 0.8 Shore A) with lower filler content.

Figure 8b–d shows the results of dynamic mechanical tests of BR/CR nanocomposites, and Table 4 summarizes the dynamic mechanical results. G' at 25°C is plotted over filler content in Figure 8b. It shows the same trend as Young's modulus: the replacement of CB or ATH by MLG and the addition of ATH caused an increase in storage modulus values. Substituting 15 phr CB with 3 phr MLG increased G' by 23% for BR/CR/MLG3/CB5 and by 42% for BR/CR/ATH50/MLG3/CB5. Adding 50 phr ATH resulted in the greatest increases in storage moduli: an increase of 287% was observed for BR/CR/ATH50/CB20 and of 346% for BR/CR/ATH50/MLG3/CB5, compared to their ATH-free equivalents. Replacing 3 phr ATH by 3 phr MLG resulted in the highest value of storage modulus (27.95 MPa) with an increase of 112%.

The storage modulus (G') is plotted as a function of temperature in Figure 8c. G' values were enhanced by the incorporation of MLG and ATH in the BR/CR matrix. An increase of storage modulus is more important above the glass transition temperature (T_g) because the rubber becomes less stiff and more viscoelastic. The substitution of CB with MLG enhanced G' thanks to the formation of a filler network in the matrix, making the rubber nanocomposites more elastic.

Figure 8d presents the damping factor (tan δ) as a function of temperature. The reduction of tan δ was observed when MLG replaced CB or ATH and when ATH was added to the rubbers. This behavior is linked to the rubber–filler interactions which restrained the elastomeric chain mobility (48,49). The diminution of tan δ also illustrates the good filler dispersion in the elastomer's matrix (50). This is supported by SEM and TEM investigations, where a good filler dispersion was visible. The substitution of CB by MLG resulted in a 6% diminution of tan δ for BR/CR/MLG3/CB5, highlighting the

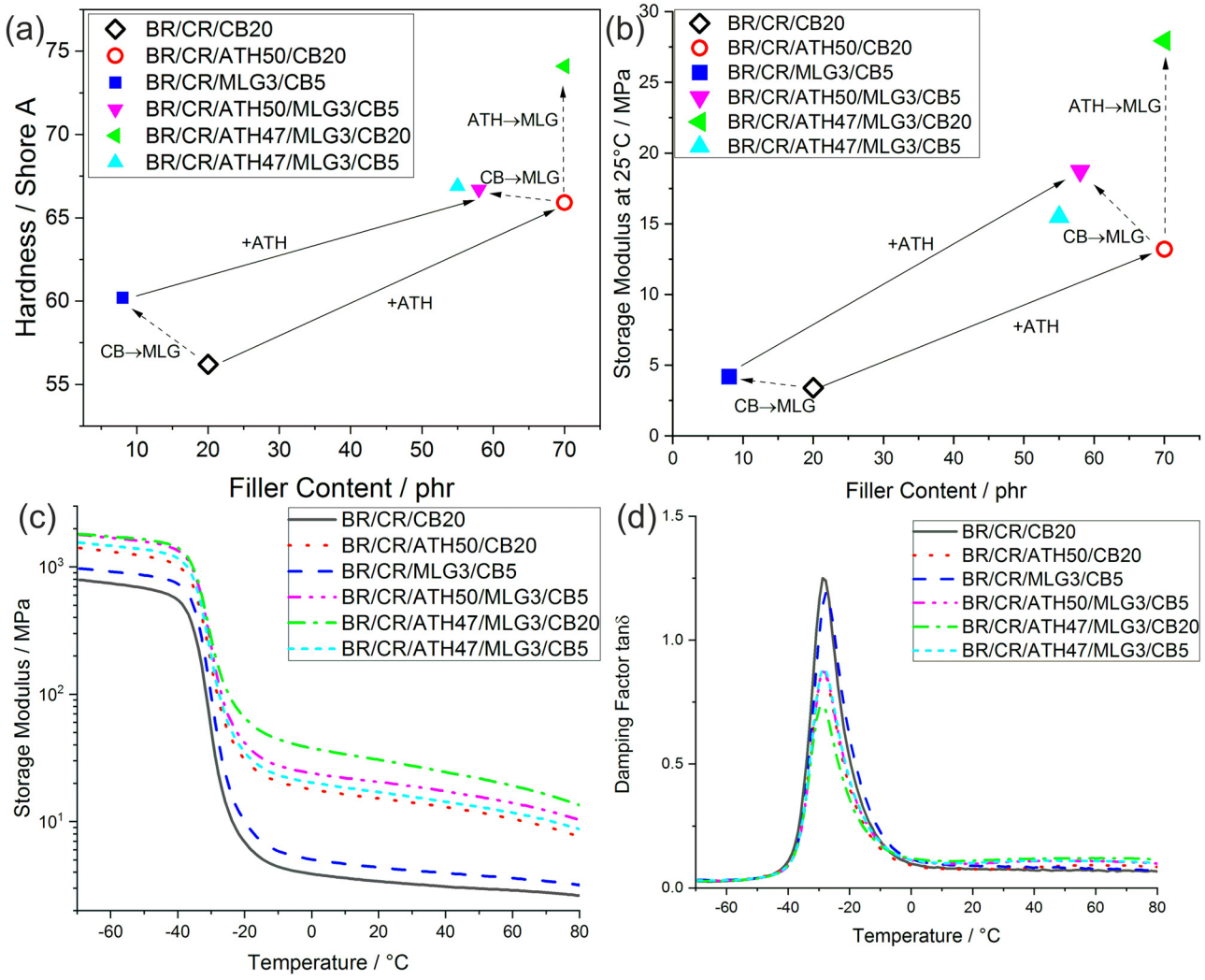

Figure 8: Hardness and dynamic mechanical results of BR/CR nanocomposites; (a) hardness in Shore A, (b) storage modulus (G') and (c) damping factor (tan δ) as a function of temperature, and (d) storage modulus at 25°C as a function of filler content. Solid line is addition of 50 phr ATH; dashed line is replacement of 15 phr CB with 3 phr MLG, or 3 phr ATH with 3 phr MLG, respectively.

Table 4: Storage modulus (G') values at −60°C, 25°C, and 50°C, maximum damping factor peak (tan δ), and the glass transition temperature (T_g) of BR/CR nanocomposites

	BR/CR/CB20	BR/CR/ATH50/CB20	BR/CR/MLG3/CB5	BR/CR/ATH50/MLG3/CB5	BR/CR/ATH47/MLG3/CB20	BR/CR/ATH47/MLG3/CB5
G' at −60°C (MPa)	752 ± 10	1,335 ± 15	949 ± 30	1,725 ± 35	1,825 ± 95	1,530 ± 60
G' at 25°C (MPa)	3.4 ± 0.1	13.2 ± 1.5	4.2 ± 0.1	18.8 ± 1.0	28.0 ± 1.3	15.5 ± 0.9
G' at 50°C (MPa)	3.1 ± 0.1	10.9 ± 0.9	3.7 ± 0.1	15.3 ± 0.5	21.5 ± 0.4	12.6 ± 0.4
max (tan δ)	1.3 ± 0.1	0.9 ± 0.1	1.2 ± 0.1	0.9 ± 0.1	0.8 ± 0.1	0.9 ± 0.1
T_g (°C)	−29.1 ± 0.3	−28.8 ± 0.1	−27.8 ± 0.1	−28.8 ± 0.1	−28.8 ± 0.1	−28.8 ± 0.1

stronger interaction between MLG and the rubber matrix. This behavior was not visible when MLG replaced CB with 50 phr ATH, because the MLG–rubber interactions were inhibited by the high amount of FR. BR/CR/ATH50/CB20, BR/CR/ATH50/MLG3/CB5, and BR/CR/ATH47/MLG3/CB5 reached the same tan δ maximum and the curves displayed the same behavior. When 3 phr ATH were replaced by 3 phr MLG with a high amount of CB, a 17% decrease in

tan δ was observed, again highlighting the synergetic effect of ATH, MLG, and CB in considerable quantities. The incorporation of 50 phr ATH decreased tan δ by more than 20%, i.e., 25% for BR/CR/ATH50/MLG3/CB5 and 29% for BR/CR/ATH50/CB20. All rubber nanocomposites displayed nearly identical glass transition temperatures: T_g was not affected by the filler content.

3.6 Mechanical properties of BR/CR rubber composites: electrical volume resistivity

Figure 9 shows the electrical volume resistivity of the rubber mixtures as a function of filler content. The addition of 3 phr MLG, in replacement of 15 phr CB or 3 phr ATH, resulted in a drastic decrease of resistivity. This is explained by the incorporation of MLG particles which form a network in the elastomeric matrix and are more conductive than ATH and CB (51). Generally, the introduction of ATH increased resistivity, as ATH acts as a poor electrical conductor. Its addition to BR/CR/CB20 increased conductivity by 159% and by 465% for BR/CR/MLG3/CB5. Compared to BR/CR/CB20 and BR/CR/ATH50/CB20, replacing CB by MLG caused a decrease in resistivity of 92% and 82% in BR/CR/MLG3/CB5 and BR/CR/ATH50/MLG3/CB5, respectively. When MLG replaced CB, the reduction of conductivity was less pronounced when ATH was present. The substitution of ATH by MLG resulted in the most significant reduction of resistivity (99% reduction) for the sample BR/CR/ATH47/MLG3/CB5, highlighting the multifunctional quality of MLG to afford good conduction properties to rubbers with high resistivity.

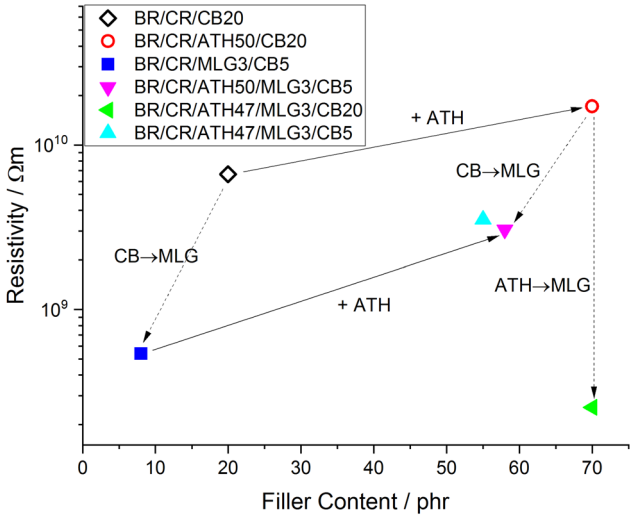

Figure 9: Electrical resistivity of BR/CR composites as a function of filler content. Solid line is addition of 50 phr ATH; dashed line is replacement of 15 phr CB with 3 phr MLG, or 3 phr ATH with 3 phr MLG, respectively.

3.7 Reaction-to-small-flame: LOI and UL-94

The LOI is used to measure the lowest oxygen concentration needed to maintain the combustion of a rubber sample lit from the top in a vertical orientation. UL-94 burning chamber measures either the vertical upward flame spread of a sample lit from the bottom or the horizontal flame spread. Table 5 summarizes LOI and UL-94 results for the BR/CR rubber composites, and Figure 10 displays the LOI values plotted over the filler content of the rubber composites. Notably, the oxygen index of BR/CR/MLG3/CB5 was higher by about 2 vol% compared to BR/CR/CB20, which is a small but significant change, as the former has a higher filler-to-rubber ratio. The addition of ATH to these two BR/CR samples increased the LOIs between 6 and 7 vol%, respectively. ATH acts as an FR through its endothermic decomposition, thus cooling the condensed phase, and by releasing water in the gas phase, thereby diluting the fuel released during combustion (34). As ATH is the main FR, the mixture BR/CR/ATH50/CB20 may be considered the control sample for assessing the synergistic effect of the other components. In Figure 10, when comparing BR/CR/ATH50/MLG3/CB5 (filler content: 58 phr) and BR/CR/ATH47/MLG3/CB20 (filler content: 70 phr), the LOIs remained at about 33 vol%, yet the mixture BR/CR/ATH47/MLG3/CB5 (filler content 55 phr) exhibited an LOI of 38 vol%, which

Table 5: LOI and UL-94 results for BR/CR composites

	BR/CR/CB20	BR/CR/ATH50/CB20	BR/CR/MLG3/CB5	BR/CR/ATH50/MLG3/CB5	BR/CR/ATH47/MLG3/CB20	BR/CR/ATH47/MLG3/CB5
LOI (vol%)	24.9 ± 0.1	31.9 ± 0.2	27.0 ± 0.2	32.9 ± 0.2	32.8 ± 0.2	38.4 ± 0.4
UL-94	NC	V-0	NC	V-0	V-0	V-0

NC – not classified.

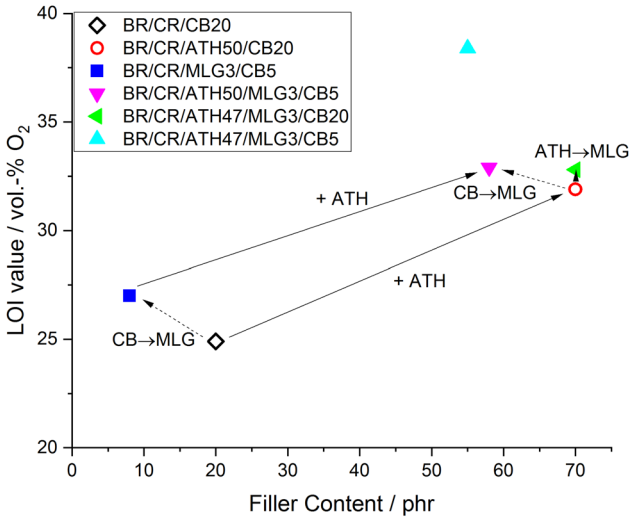

Figure 10: LOI values plotted over filler content. Solid line is addition of 50 phr ATH; dashed line is replacement of 15 phr CB with 3 phr MLG, or 3 phr ATH with 3 phr MLG, respectively.

was significantly increased compared to all other materials. All flame-retarded blends containing ATH and MLG exhibited higher LOIs than the control sample BR/CR/ATH50/CB20. The mixture of ATH, MLG, CB, and BR/CR in this ratio presented very good reaction-to-small-flame behavior, potentially due to synergism between these components.

The LOI results are in line with the UL-94 results, where all ATH-containing materials exhibited V-0 classification. The use of ATH prevented the vertical flame propagation, whereas the non-flame retarded samples were not classified.

3.8 Forced flaming fire behavior: cone calorimeter

Cone calorimeter measurements are central to characterize the fire and flame retardancy behavior of a polymeric material. Figure 11 displays the heat release rate (HRR) curves (Figure 11a), the total heat release (THR) curves (Figure 11b), and the mass loss curves (Figure 11) of the BR/CR rubbers over time, while the Petrella plot is shown in Figure 11d. Petrella plots are a useful way to visualize fire hazard by plotting the fire load against an index for flame spread (52). The HRR curves in Figure 11a make clear that non-flame retarded formulations ignited more quickly than the flame retarded ones. All ATH-containing formulations exhibited a very strong protective layer effect exemplified by the strong decrease of peak of HRR (PHRR) compared to non-ATH containing samples. The decomposition of ATH leads to the release of water and the formation of Al_2O_3 aluminum oxide (34), creating a protective layer at the specimen's surface. The HRR curves of ATH-containing specimens are characteristic of a thermally thick charring material, with an additional peak at the end of burning caused by the cracking of the protective layer (53). Contrarily, those samples without ATH exhibited a thermally thin, non-charring HRR curve: after ignition, the material easily volatized and quickly reached its PHRR. Therefore, the PHRR for flame retarded formulations are lowered by a factor of 4 when compared to non-flame retarded ones, where the PHRRs were over 800 kW m^{-2} for BR/CR/CB20 and BR/CR/MLG3/CB5 (Table 6).

The addition of ATH to BR/CR/CB20 and BR/CR/MLG3/CB5 improved the time to ignition (t_{ig}) by 8 and 17 s, respectively, which was expected due to the FR properties of ATH. Contrarily, the replacement of 15 phr CB with 3 phr MLG for BR/CR/MLG3/CB5 caused a decrease of t_{ig} by 7 s and an overall increase in mass loss, caused by the increased ratio of combustible BR/CR to filler content. Thus, ATH was the main contributor to lowering PHRR, t_{ig}, mass loss, and smoke production. Thus, the blend BR/CR/ATH50/CB20 represents a benchmark sample to investigate the effects of MLG. Interestingly, when the combination of ATH and MLG was adjusted, e.g., in BR/CR/ATH47/MLG3/CB5, an improved or equal t_{ig} and PHRR were observed compared to BR/CR/ATH50/CB20. This result highlights that the combination of ATH and MLG had a constructive effect on improving the fire properties of BR/CR and that by adding MLG to ATH formulations, up to 15 phr of filler could be replaced. This effect is related to a synergic effect of MLG, ATH, and CB in high filler contents: MLG dissipates the heat into the specimen (51), ATH dilutes the flammable gases by releasing water (34), and CB in high amounts delays the material's combustion due to the reduction of combustible BR/CR fuel. These effects vary depending on the ratios of ATH:MLG:CB, as BR/CR/ATH47/MLG3/CB20 exhibited a higher t_{ig} than BR/CR/ATH47/MLG3/CB5 due to the lower rubber content, yet the former exhibited a higher PHRR than the latter due to the decreased protection layer, potentially from the increased CB content affecting the char residue morphology. The ratio of ATH:MLG:CB affected the varying fire scenarios, as BR/CR/ATH47/MLG3/CB5 attained a substantially higher LOI value than BR/CR/ATH47/MLG3/CB20, indicating that it had better protection against small

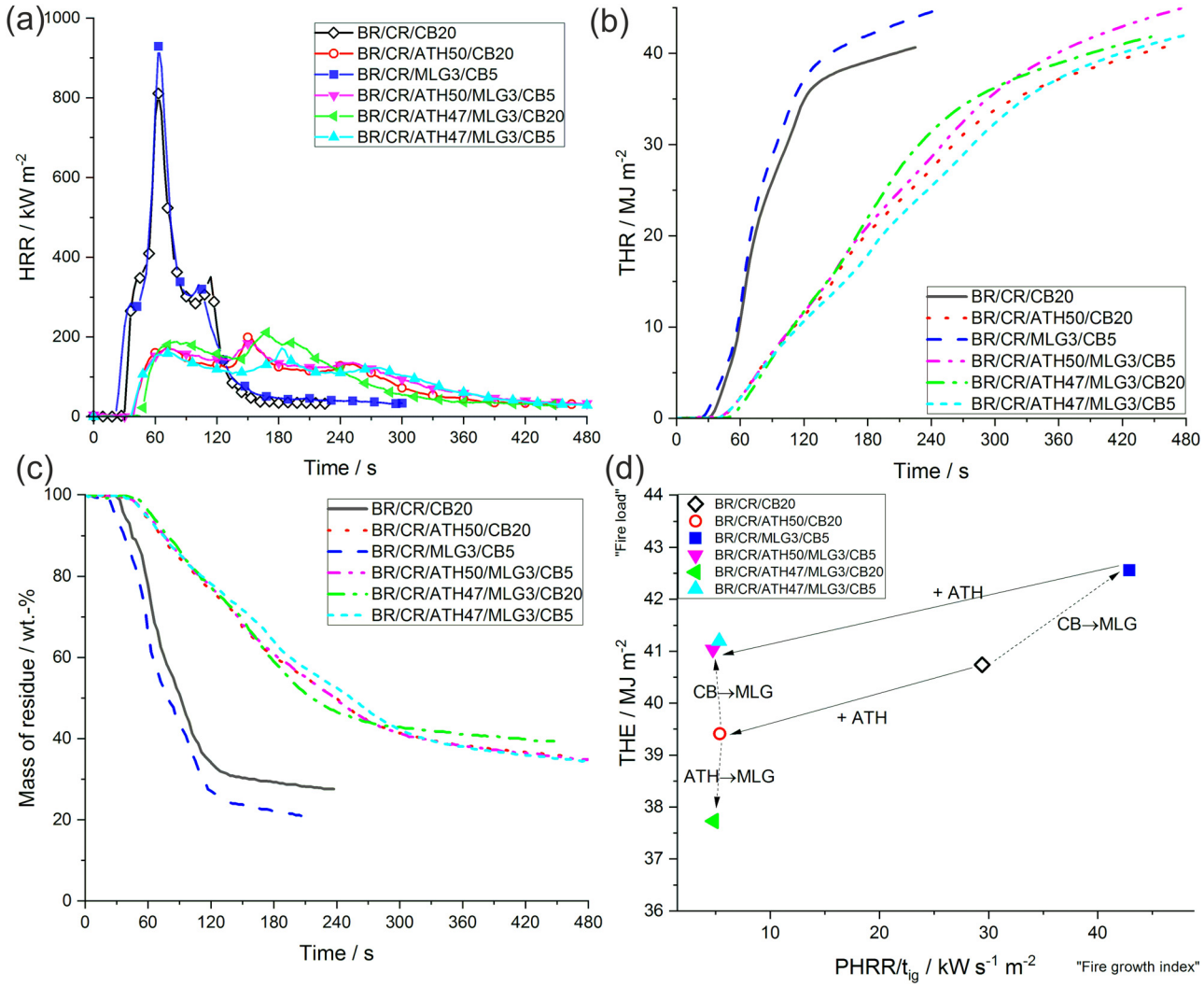

Figure 11: (a) HRR, (b) THR, (c) mass of residue, and (d) THE of the BR/CR composites as a function of time.

Table 6: Cone calorimeter results of BR/CR nanocomposites

	BR/CR/CB20	BR/CR/ATH50/CB20	BR/CR/MLG3/CB5	BR/CR/ATH50/MLG3/CB5	BR/CR/ATH47/MLG3/CB20	BR/CR/ATH47/MLG3/CB5
PHRR (kW m^{-2})	822 ± 11	193 ± 6	901 ± 28	180 ± 5	212 ± 1	189 ± 17
THE (MJ m^{-2})	40.7 ± 1.7	39.4 ± 0.8	42.6 ± 0.2	41.0 ± 1.9	37.7 ± 1.2	41.2 ± 1.7
t_{ig} (s)	28 ± 1	36 ± 1	21 ± 0	38 ± 1	44 ± 0	36 ± 1
Mass loss (%)	71 ± 0	63 ± 0	76 ± 0	63 ± 0	58 ± 0	64 ± 0
EHC (MJ kg^{-1})	15.5 ± 0.6	15.0 ± 0.2	15.5 ± 0.1	15.9 ± 0.7	15.2 ± 0.3	15.9 ± 0.6
FIGRA (kW m^{-2} s^{-1})	12.7 ± 0.1	2.7 ± 0.0	14.3 ± 0.4	2.5 ± 0.1	2.6 ± 0.1	2.7 ± 0.1
MARHE (kW m^{-2})	306 ± 14	119 ± 4	328 ± 9	114 ± 7	129 ± 3	115 ± 7
TSP (m^2 m^{-2})	3,923 ± 89	3,053 ± 85	4,095 ± 106	2,987 ± 89	3,063 ± 26	3,070 ± 57

flames, yet the latter exhibited a lower fire load in forced flaming combustion.

Figure 11b displays the THR as a function of time. From the curves' profile, it is observed that ATH-free rubbers quickly reached higher THR values compared to formulations containing ATH. Replacing 15 phr CB with 3 phr MLG resulted in slightly higher THR over time, both for flame retarded and non-flame retarded

nanocomposites. This behavior was caused by the decreased filler content, causing the content of rubber, i.e., combustible fuel, to be higher. The total heat evolved (THE) is determined from the THR value at flame out and represents the specimen's fire load. The substitution of 15 phr CB with 3 phr MLG improved the fire load by 4% for both BR/CR/CB20 and BR/CR/ATH50/CB20. The addition of 50 phr ATH slightly decreased THE by 3% and 4% for BR/CR/CB20 and BR/CR/MLG3/CB5, respectively. This was the result of ATH affecting the combustion efficiency of the flame, thereby retaining more fuel in the condensed phase. The substitution of 3 phr ATH by 3 phr MLG resulted in the lowest value of THE, indicating that MLG, CB, and ATH showed good synergistic tendencies in this formulation. The effective heat of combustion (EHC) is the ratio of THE to total mass loss and is an indicator for gas phase activity (54), particularly flame poisoning. EHC is neither affected by the substitution of CB or ATH with MLG nor the addition of ATH since all the formulations had the same range of values.

Figure 11c exhibits the sample mass as a function of time. Mass loss occurs in a narrower time frame and in a more pronounced manner for non-flame retarded rubbers: adding ATH delayed the mass loss of the material and slowed down the specimen decomposition. The replacement of 15 phr CB with 3 phr MLG accelerated mass loss and led to a lower mass residue due to the diminution of filler content and the good conductivity of MLG compared to CB. The same replacement in the presence of 50 phr ATH did not change the curve's shape and reached the same mass loss value despite the difference in filler content, showing that ATH had the same flame-retardant behavior toward CB20 and MLG3/CB5. The substitution of 3 phr ATH by 3 phr MLG led to a slightly higher mass residue but the two curves have the same behavior during the first 2 min.

The FIGRA (fire growth rate) and MARHE (maximum average rate of heat emission) indices help to evaluate flame spread. FIGRA stems from EN 13823 for building products and is used for single burning item tests; it is calculated as the maximum of (HRR/t). MARHE is used for cone calorimeter tests with respect to fire protection railway vehicles (CEN TS 45545). Replacing 15 phr CB with 3 phr MLG enhanced FIGRA by 11% due to the conductive behavior of MLG. The addition of ATH reduced the rubbers' FIGRA and led to similar values regardless of rubber formulation (around 2.6 kW m^{-2} s^{-1}): when adding 50 phr ATH, declines of 79% and 83% were observed for BR/CR/CB20 and BR/CR/MLG3/CB5, respectively. ATH addition reduced MAHRE by more than 60% compared to ATH-free rubbers. All flame retarded formulations reached the same MAHRE value, except when 3 phr MLG substituted 3 phr ATH: an increase of 8% was observed. The replacement of 15 phr CB with 3 phr MLG enhanced MARHE by 7% for BR/CR/CB20 and had no influence for BR/CR/ATH50/CB20.

The impact of ATH on the total smoke production (TSP) of the BR/CR mixtures highlights the important role of FRs for rubbers. In particular, elastomers are widely used in public transportation; in a fire scenario, the dense smoke production associated with rubber fires is a particular danger that can severely hamper escape times due to poor visibility and increase health risks due to smoke inhalation. The addition of ATH in rubber formulations decreased TSP by about a quarter, from about 4,000 m^2 m^{-2} for non ATH-containing rubbers to about 3,000 m^2 m^{-2} for ATH-containing formulations. Interestingly, the replacement of 3 phr ATH with MLG did not greatly affect the decreased smoke production; in fact, the formulation where MLG replaced 3 phr ATH and 15 phr CB had similar levels of smoke production to those mixtures with higher filler contents. The results highlight the ability of MLG to replace CB and even ATH without sacrificing smoke hampering effects.

The Petrella plot is used to assess composites' fire hazard development. THE is plotted against PHRR/t_{ig} in Figure 11d, in which THE represents the fire load and PHRR/t_{ig} the fire growth index. It is observed that substituting 15 phr CB by 3 phr MLG increased not only the fire load but also the fire growth index regarding non-flame retarded nanocomposites. The addition of 50 phr ATH resulted in a drastic decrease of fire growth index (89% for BR/CR/MLG3/CB5 and 82% for BR/CR/CB20) and a diminution of the fire load. Replacing 3 phr ATH by 3 phr MLG affected the fire load but left the fire growth index intact, showing once more the synergic effect of MLG, ATH, and CB in high loading.

Figure 12 presents the sample residues of the BR/CR nanocomposites obtained after cone calorimeter measurements. The formulations containing CB, MLG, and ATH conserved their shape after burning, whereas the other formulations were more brittle and broke more easily. In particular, the formulation of BR/CR/ATH50/CB20 was particularly brittle due to the high ATH content. The addition of MLG into the rubber mixtures allowed the material to retain its shape without comprising the fire performance. In particular, in the application of rubbers as sealants or particularly BR/CR for tires, maintaining shape and perhaps some structural properties in the process certainly increases the safety of the material.

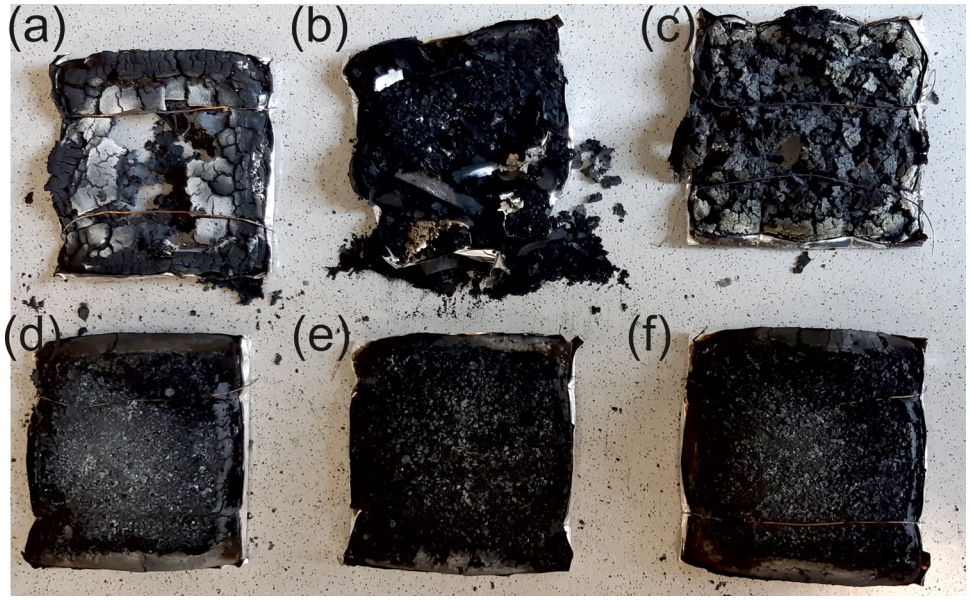

Figure 12: Sample residues after cone calorimeter measurements. (a) BR/CR/CB20, (b) BR/CR/ATH50/CB20, (c) BR/CR/MLG3/CB5, (d) BR/CR/ATH50/MLG3/CB5, (e) BR/CR/ATH47/MLG3/CB20, and (f) BR/CR/ATH47/MLG3/CB5.

4 Conclusion

The aim of this study was to investigate MLG in BR/CR mixtures. The rubber mixtures were formulated to investigate the substitution of ATH and of CB with MLG. Investigating the mechanical properties highlighted that mixtures where MLG replaced 3 phr ATH (with 20 phr CB) exhibited higher storage moduli, higher maximum torque, increased Young's moduli, and increased shore hardness. Moreover, the replacement of ATH and CB with MLG led to increased flame retardancy of BR/CR, as an LOI of 38.4 vol% was reached by BR/CR/ATH47/MLG3/CB5. Additionally, the incorporation of MLG into ATH-containing rubbers led to a better fire behavior, as BR/CR/ATH47/MLG3/CB20 exhibited the lowest fire load and FIGRA. 3 phr MLG was able to replace 15 phr CB in terms of mechanical and flame retardancy properties, and in many cases, the replacement of both 3 phr ATH and 15 phr CB by 3 phr MLG led to nearly no change in material properties. The use of MLG as a replacement of up to 18 phr of additives to rubber signifies its multifunctional qualities as a filler to BR/CR mixtures: MLG displays reinforcing effects and its ability to reduce fire loads and FIGRAs make it attractive to partially reduce ATH contents, particularly without sacrificing smoke hampering effects or increasing MARHE or FIGRA. MLG has been proven effective in several rubber matrices previously, and this study shows that MLG can effectively lower filler contents in BR/CR rubbers without greatly affecting mechanical properties or fire behavior.

Acknowledgements: The authors sincerely thank Bettina Strommer for TEM measurements, Patrick Klack for aid with the cone calorimeter, Christian Huth for DMA measurements, and Bernd Krafft for his help in preparing the rubber composites. Many thanks to Mr. Feher of Graphit Kropfmühl AG for supplying MLG and to Nabaltec AG for supplying ATH.

Research funding: The authors state no funding involved.

Author contributions: Alexander Battig: writing – original draft, writing – review and editing, investigation, formal analysis, visualization, and project administration; Naïssa Abdou-Rahaman Fadul: writing – original draft, visualization, investigation, and formal analysis; Daniele Frasca: conceptualization, methodology, investigation, formal analysis, visualization, and resources; Dietmar Schulze: investigation, formal analysis, methodology, data curation, and resources; Bernhard Schartel: writing – review and editing, conceptualization, project administration, and supervision.

Conflict of interest: The authors declare no conflict of interest.

Data availability statement: Data are available upon request.

References

(1) Wolff S. Chemical aspects of rubber reinforcement by fillers. Rubber Chem Technol. 1996;69(3):325–46. doi: 10.5254/1.3538376.

(2) Arrighi V, McEwen I, Qian H, Prieto MS. The glass transition and interfacial layer in styrene-butadiene rubber containing silica nanofiller. Polymer. 2003;44(20):6259–66. doi: 10.1016/S0032-3861(03)00667-0.

(3) Böhning M, Frasca D, Schulze D, Schartel B. Multilayer graphene/elastomer nanocomposites. In: Yaragalla S, Mishra RK, Thomas S, Kalarikkal N, Maria H, editors. Chapter: 6. Carbon-based nanofiller and their rubber nanocomposites. Elsevier; 2019.

(4) Arroyo M, López-Manchado MA, Herrero B. Organo-montmorillonite as substitute of carbon black in natural rubber compounds. Polymer. 2003;44(8):2447–53. doi: 10.1016/S0032-3861(03)00090-9.

(5) Ali Z, Le HH, Ilisch S, Thurn-Albrecht T, Radusch H-J. Morphology development and compatibilization effect in nanoclay filled rubber blends. Polymer. 2010;51(20):4580–8. doi: 10.1016/j.polymer.2010.08.002.

(6) Gallo E, Schartel B, Schmaucks G, Von der Ehe K, Böhning M. Effect of well dispersed amorphous silicon dioxide in flame retarded styrene butadiene rubber. Plast Rubber Compos. 2013;42(1):34–42. doi: 10.1179/1743289812Y.0000000012.

(7) Yang H, Zhang X, Qu C, Li B, Zhang L, Zhang Q, et al. Largely improved toughness of PP/EPDM blends by adding nano-SiO_2 particles. Polymer. 2007;48:860–9. doi: 10.1016/j.polymer.2006.12.022.

(8) Bokobza L. The reinforcement of elastomeric networks by fillers. Macromol Mater Eng. 2004;289(7):607–21. doi: 10.1002/mame.200400034.

(9) Bai L, Bai Y, Zheng J. Improving the filler dispersion and performance of silicone rubber/multi-walled carbon nanotube composites by noncovalent functionalization of polymethylphenylsiloxane. J Mater Sci. 2017;52(12):7516–29. doi: 10.1007/s10853-017-0984-y.

(10) Beckert F, Trenkle S, Thomann R, Mülhaupt R. Mechanochemical route to functionalized graphene and carbon nanofillers for graphene/SBR nanocomposites. Macromol Mater Eng. 2014;299(12):1513–20. doi: 10.1002/mame.201400205.

(11) Das A, Kasaliwal GR, Jurk R, Boldt R, Fischer D, Stöckelhuber KW, et al. Rubber composites based on graphene nanoplatelets, expanded graphite, carbon nanotubes and their combination: a comparative study. Compos Sci Technol. 2012;72(16):1961–7. doi: 10.1016/j.compscitech.2012.09.005.

(12) Schopp S, Thomann R, Ratzsch K-F, Kerling S, Altstädt V, Mülhaupt R. Functionalized graphene and carbon materials as components of styrene-butadiene rubber nanocomposites prepared by aqueous dispersion blending. Macromol Mater Eng. 2014;299(3):319–29. doi: 10.1002/mame.201300127.

(13) Joo H, Han H, Cho S. Fabrication of poly(vinyl alcohol)-polyaniline nanofiber/graphene hydrogel for high-performance coin cell supercapacitor. Polymers. 2020;12(4):928.

(14) Burk L, Gliem M, Lais F, Nutz F, Retsch M, Mülhaupt R. Mechanochemically carboxylated multilayer graphene for carbon/ABS composites with improved thermal conductivity. Polymers. 2018;10(10):1088. doi: 10.3390/polym10101088.

(15) Frasca D, Schulze D, Wachtendorf V, Huth C, Schartel B. Multifunctional multilayer graphene/elastomer nanocomposites. Eur Polym J. 2015;7199–113. doi: 10.1016/j.eurpolymj.2015.07.050.

(16) Frasca D, Schulze D, Böhning M, Krafft B, Schartel B. Multilayer graphene chlorine isobutyl isoprene rubber nanocomposites: influence of the multilayer graphene concentration on physical and flame-retardant properties. Rubber Chem Technol. 2016;89(2):316–34. doi: 10.5254/rct.15.84838.

(17) Frasca D, Schulze D, Wachtendorf V, Morys M, Schartel B. Multilayer graphene/chlorine-isobutene-isoprene rubber nanocomposites: the effect of dispersion. Polym Adv Technol. 2016;27(7):872–81. doi: 10.1002/pat.3740.

(18) Frasca D, Schulze D, Wachtendorf V, Krafft B, Rybak T, Schartel B. Multilayer graphene/carbon black/chlorine isobutyl isoprene rubber nanocomposites. Polymers. 2016;8(3):95. doi: 10.3390/polym8030095.

(19) Zirnstein B, Tabaka W, Frasca D, Schulze D, Schartel B. Graphene/hydrogenated acrylonitrile-butadiene rubber nanocomposites: dispersion, curing, mechanical reinforcement, multifunctional filler. Polym Test. 2018;66268–79. doi: 10.1016/j.polymertesting.2018.01.035.

(20) Valentini L, Lopez-Manchado MA. Classification of rubbers and components for harsh environmental systems. In: Valentini L, Lopez-Manchado MA, editors. High-performance elastomeric materials reinforced by nano-carbons. Amsterdam: Elsevier; 2020.

(21) Obrecht W, Lambert J-P, Happ M, Oppenheimer-Stix C, Dunn J, Krüger R. Rubber, 4. Emulsion rubbers. In: Elvers B, editor. Chapter: 4. Ullmann's encyclopedia of industrial chemistry. Chichester, John Wiley & Sons; 2011.

(22) Polybutadiene market by type (solid polybutadiene (high cis, low cis, high trans, high vinyl), liquid polybutadiene), application (tires, polymer modification, industrial rubber, chemical), and region - global forecast to 2024. Markets and Markets; 2019.

(23) Neoprene market: global industry trends, share, size, growth, opportunity and forecast 2020–2025. IMARC Market Research; 2019.

(24) Dittrich B, Wartig K-A, Hofmann D, Mülhaupt R, Schartel B. Carbon black, multiwall carbon nanotubes, expanded graphite and functionalized graphene flame retarded polypropylene nanocomposites. Polym Adv Technol. 2013;24(10):916–26. doi: 10.1002/pat.3165.

(25) Steurer P, Wissert R, Thomann R, Mülhaupt R. Functionalized graphenes and thermoplastic nanocomposites based upon expanded graphite oxide. Macromol Rapid Commun. 2009;30(4–5):316–27. doi: 10.1002/marc.200800754.

(26) Dittrich B, Wartig KA, Mulhaupt R, Schartel B. Flame-retardancy properties of intumescent ammonium poly(phosphate) and mineral filler magnesium hydroxide in combination with graphene. Polymers. 2014;6(11):2875–95. doi: 10.3390/polym6112875.

(27) Gilman JW, Kashiwagi T. Polymer-layered silicate nanocomposites with conventional flame retardants. In: Pinnavaia T, Beall G, editors. Chapter: 10. Polymer-clay nanocomposites. Chichester: John Wiley & Sons; 2000.

(28) He W, Song P, Yu B, Fang Z, Wang H. Flame retardant polymeric nanocomposites through the combination of nanomaterials and conventional flame retardants. Prog Mater Sci. 2020;100687. doi: 10.1016/j.pmatsci.2020.100687.
(29) Lopez-Cuesta J-M, Laoutid F, Multicomponent FR. Systems: polymer nanocomposites combined with additional materials. In: Wilkie CA, Morgan AB, editors. Chapter: 12. Fire retardancy of polymeric materials. Boca Raton, FL: CRC Press; 2010.
(30) Bourbigot S, Duquesne S, Fontaine G, Bellayer S, Turf T, Samyn F. Characterization and reaction to fire of polymer nanocomposites with and without conventional flame retardants. Mol Cryst Liq Cryst. 2008;4861367–81. doi: 10.1080/15421400801921983.
(31) Schartel B, Knoll U, Hartwig A, Pütz D. Phosphonium-modified layered silicate epoxy resins nanocomposites and their combinations with ATH and organo-phosphorus fire retardants. Polym Adv Technol. 2006;17(4):281–93. doi: 10.1002/pat.686.
(32) Wu Z-H, Zhou B, Fan Q-X, Cai Y-J. Thermal degradation kinetics investigation on Nano-ZnO/IFR synergetic flame retarded polypropylene/ethylene-propylene-diene monomer composites processed via different fields. E-Polymers. 2019;19(1):50–60. doi: 10.1515/epoly-2019-0007.
(33) Lu F-L, Shen M-X, Xue Y-J, Zeng S-H, Chen S-N, Hao L-Y, et al. Application of calcium montmorillonite on flame resistance, thermal stability and interfacial adhesion in polystyrene nanocomposites. E-Polymers. 2019;19(1):92–102. doi: 10.1515/epoly-2019-0012.
(34) Hull TR, Witkowski A, Hollingbery L. Fire retardant action of mineral fillers. Polym Degrad Stab. 2011;96(8):1462–9. doi: 10.1016/j.polymdegradstab.2011.05.006.
(35) Schartel B, Bartholmai M, Knoll U. Some comments on the use of cone calorimeter data. Polym Degrad Stab. 2005;88(3):540–7. doi: 10.1016/j.polymdegradstab.2004.12.016.
(36) Xing W, Wu J, Huang G, Li H, Tang M, Fu X. Enhanced mechanical properties of graphene/natural rubber nanocomposites at low content. Polym Int. 2014;63(9):1674–81. doi: 10.1002/pi.4689.
(37) Payne AR. The dynamic properties of carbon black-loaded natural rubber vulcanizates. Part I. J Appl Polym Sci. 1962;6(19):57–63. doi: 10.1002/app.1962.070061906.
(38) Coran A. Chemistry of the vulcanization and protection of elastomers: a review of the achievements. J Appl Polym Sci. 2003;87(1):24–30. doi: 10.1002/app.11659.
(39) Teh PL, Mohd Ishak ZA, Hashim AS, Karger-Kocsis J, Ishiaku US. Effects of epoxidized natural rubber as a compatibilizer in melt compounded natural rubber–organoclay nanocomposites. Eur Polym J. 2004;40(11):2513–21. doi: 10.1016/j.eurpolymj.2004.06.025.
(40) Zhan Y, Wu J, Xia H, Yan N, Fei G, Yuan G. Dispersion and exfoliation of graphene in rubber by an ultrasonically-assisted latex mixing and *in situ* reduction process. Macromol Mater Eng. 2011;296(7):590–602. doi: 10.1002/mame.201000358.
(41) Malas A, Pal P, Das CK. Effect of expanded graphite and modified graphite flakes on the physical and thermomechanical properties of styrene butadiene rubber/polybutadiene rubber (SBR/BR) blends. Mater Des. 2014;55664–73. doi: 10.1016/j.matdes.2013.10.038.
(42) Ismail H, Chia HH. The effects of multifunctional additive and vulcanization systems on silica filled epoxidized natural rubber compounds. Eur Polym J. 1998;34(12):1857–63. doi: 10.1016/S0014-3057(98)00029-9.
(43) Ismail H, Chia HH. The effects of multifunctional additive and epoxidation in silica filled natural rubber compounds. Polym Test. 1998;17(3):199–210. doi: 10.1016/S0142-9418(97)00043-3.
(44) Verdejo R, Bernal MM, Romasanta LJ, Lopez-Manchado MA. Graphene filled polymer nanocomposites. J Mater Chem. 2011;21(10):3301–10. doi: 10.1039/c0jm02708a.
(45) Malas A, Das CK, Das A, Heinrich G. Development of expanded graphite filled natural rubber vulcanizates in presence and absence of carbon black: mechanical, thermal and morphological properties. Mater Des. 2012;39410–7. doi: 10.1016/j.matdes.2012.03.007.
(46) Song S, Jeong H, Kang Y. Preparation and characterization of exfoliated graphite and its styrene butadiene rubber nanocomposites. J Ind Eng Chem. 2010;16(6):1059–65. doi: 10.1016/j.jiec.2010.07.004.
(47) Schartel B, Wendorff JH. Molecular composites for molecular reinforcement: a promising concept between success and failure. Polym Eng Sci. 1999;39(1):128–51. doi: 10.1002/pen.11403.
(48) Poikelispää M, Das A, Dierkes W, Vuorinen J. The effect of partial replacement of carbon black by carbon nanotubes on the properties of natural rubber/butadiene rubber compound. J Appl Polym Sci. 2013;130(5):3153–60. doi: 10.1002/app.39543.
(49) Menes O, Cano M, Benedito A, Giménez E, Castell P, Maser WK, et al. The effect of ultra-thin graphite on the morphology and physical properties of thermoplastic polyurethane elastomer composites. Compos Sci Technol. 2012;72(13):1595–601. doi: 10.1016/j.compscitech.2012.06.016.
(50) Potts JR, Shankar O, Murali S, Du L, Ruoff RS. Latex and two-roll mill processing of thermally-exfoliated graphite oxide/natural rubber nanocomposites. Compos Sci Technol. 2013;74166–72. doi: 10.1016/j.compscitech.2012.11.008.
(51) Dittrich B, Wartig K-A, Hofmann D, Mülhaupt R, Schartel B. Flame retardancy through carbon nanomaterials: carbon black, multiwall nanotubes, expanded graphite, multi-layer graphene and graphene in polypropylene. Polym Degrad Stab. 2013;98(8):1495–505. doi: 10.1016/j.polymdegradstab.2013.04.009.
(52) Petrella R. The assessment of full-scale fire hazards from cone calorimeter data. J Fire Sci. 1994;12(1):14–43. doi: 10.1177/073490419401200102.
(53) Schartel B, Hull TR. Development of fire-retarded materials – interpretation of cone calorimeter data. Fire Mater. 2007;31(5):327–54. doi: 10.1002/fam.949.
(54) Schartel B, Perret B, Dittrich B, Ciesielski M, Krämer J, Müller P, et al. Flame retardancy of polymers: the role of specific reactions in the condensed phase. Macromol Mater Eng. 2016;301(1):9–35. doi: 10.1002/mame.201500250.